Numerical simulations of the critical diameter and flame stability for hydrogen flames

International Journal of Hydrogen Energy 59 (2024) 591–603

Contents lists available at ScienceDirect

International Journal of Hydrogen Energy

journal homepage: www.elsevier.com/locate/he

Numerical simulations of the critical diameter and flame stability for hydrogen flames

M. Kazemi *, S. Brennan, V. Molkov

Hydrogen Safety Engineering and Research Centre (HySAFER) Centre, University of Ulster, Newtownabbey, BT37 0QB, UK

ARTICLE INFO

Handling editor: E.A. Veziroglu

Keywords:
Critical diameter
Blow-out
Lift-off
Attached flame
Stability limits
Hydrogen under-expanded jets

ABSTRACT

This study focuses on development and validation of a CFD model to simulate the critical nozzle diameter and stability limits for hydrogen non-premixed flames. The critical diameter represents the minimum nozzle size through which a flame will remain stable at all driving pressures. Flames will not blow-out at diameters equal to or greater than the critical diameter. Accurate simulation of this parameter is important to assess performance of thermally activated pressure relief devices (TPRD) during blowdown from a storage tank. Flame stability is considered for diameters and overpressures ranging from 0.1 mm to 2 mm and from 0.06 MPa to 20 MPa, respectively. The impact of turbulent Schmidt number Sc_t, on predicted critical diameter is discussed. The model was applied for lower pressures (0.001–0.005 MPa) to understand the pressure at which the flame becomes attached. Simulations of a safer approach to TPRD design are discussed.

1. Introduction

High-pressure gaseous hydrogen storage is the most common technology for onboard storage in automotive and rail applications as well as at stationary tanks at hydrogen refuelling stations. Where the tank or piping system is damaged, or the thermally activated pressure relief device (TPRD) opens, the hydrogen released is likely to ignite resulting in an under-expanded jet fire. Depending on the stability of the flame, blow-out may occur, potentially leading to formation of a flammable cloud, especially for releases in confined spaces [1], that can then deflagrate or even detonate with serious safety implications. The ability to numerically predict blow-out phenomenon is important from a hydrogen safety engineering perspective. As the release pressure drops during tank blowdown from storage tank, it is possible for a stable flame to blow-out and form unignited jet. Hydrogen flame may be lifted or attached to the burner dependent on driving pressure, i.e., pressure at the nozzle exit. An understanding of the pressure limits for hydrogen flames is important for inherently safer design of hydrogen systems, including TPRDs, and infrastructure.

1.1. Blow-out mechanism

The terms blow-off and blow-out have been used interchangeably in some studies, but Wu et al. [2], Messaoudani et al. [3] and Cheng et al. [4] defined blow-out as extinguishment of a lifted flame and blow-off as extinguishment of an attached flame and this definition is used here. Different models have been proposed to explain the flame stabilization mechanism. In 1965, Phillips [5] was the pioneer researcher who introduced the concept of the triple flame or edge-flame; he stated that the flame zone is partially premixed and is divided into three regions: the premixed flame, the diffusion flame separating (the fuel-rich zone from the fuel-lean zone), and the convection flame. In 1966, Vanquickenborne and Van Tiggelen [6] suggested a premixed flame propagation model to predict lift-off height and structure of turbulent diffusion flames. The flame stabilization point was defined as a distance from the burner exit where the turbulent burning velocity of the premixed flame is equal to the mean gas velocity, and blow-out occurs when the mean gas velocity exceeds the turbulent burning velocity. The premixed flame theory of Vanquickenborne and Van Tiggelen [6] was supported by Kalghatgi [7] in 1984, Kaplan et al. [8] in 1994 and Joedicke et al. [9] in 2005. In 1984, Broadwell et al. [10] proposed another stabilization mechanism for turbulent non-premixed flames, suggesting that large-scale turbulent eddies exiting from the nozzle expel hot gases to the lateral edge of the jet. Re-entrainment of the hot gases ignite the non-combusting turbulent structure in the jet. Flame stabilization occurs if the mixing time of the re-entrained hot gases is long enough, otherwise blow-out occurs. In 1996, Tieszen et al. [11] developed a correlation including the premixed flame mechanism and large-scale turbulent eddies. In 1983, Peters et al. [12] proposed another concept to describe

* Corresponding author.
E-mail address: m.kazemi@ulster.ac.uk (M. Kazemi).

https://doi.org/10.1016/j.ijhydene.2024.02.039
Received 16 June 2023; Received in revised form 11 January 2024; Accepted 3 February 2024
Available online 9 February 2024

Nomenclature

C_P	constant pressure specific heat (J/kg/K)
P	pressure (Pa)
U	velocity (m/s)
T	temperature (K)
E	total energy (J/kg)
H	enthalpy (J/kg)
g	gravity acceleration (m/s^2)
t	time (s)
Sc	Schmidt number (−)
Pr	Prandtl number (−)
Y	mass fraction (−)
D	molecular diffusivity (m^2/s)
k	turbulent kinetic energy (m^2/s^2)
τ	time scale of small-scale motions (s)
ξ	length scale of small-scale motions (−)
G_k	the production of turbulence kinetic energy due to the mean velocity gradients (kg/m/s^3)
G_b	the production of turbulence kinetic energy due to the buoyancy (kg/m/s^3)
S_{ij}	the mean rate-of-strain tensor (s^{-1})
S_E	energy source term (J/m^3/s)
S_m	source term in chemical species transport (kg/m^3/s)
R	net rate of production/destruction of species (kg/m^3/s)
r	radius (m)
L	length (m)
d	diameter (m)

Greek

ρ	density (kg/m^3)
μ	dynamic viscosity (kg/m/s)
ν	kinematic viscosity (m^2/s)
ε	energy dissipation rate (m^2/s^2)

Subscripts

i,j,k	cartesian coordinate indexes
m	chemical species
t	turbulent
E	energy
f	flame
s	surrounding
N	nozzle exit
H_2	hydrogen

Superscripts

$*$	fine-scale quantities

Constants and model parameters

$C_{1\varepsilon}$	1.44
C_2	1.9
σ_k	1.0
σ_ε	1.2
C_τ	0.4082
C_ξ	2.137

the stabilization mechanism; they state that the lift-off and blow-out are controlled by local quenching of laminar flamelets; these laminar diffusion flamelets exist at stochiometric surfaces which are very few in regions where the scalar dissipation rate is low enough for famelets to exist, consequently flamelets will be extinguished, finally reaching blow-out at sufficiently high nozzle exit velocities. In 1994, Muller et al. [13] combined both the flamelet quenching model of Peters et al. [12] and the premixed flame theory to determine flame propagation and lift-off height for turbulent jet diffusion methane flames. In 2006, Wu et al. [14] proposed blow-out occurs when the flame base is pushed downstream beyond the maximum waistline position of the stoichiometric concentration iso-surface and the flame becomes unstable. Moreover, the triple flame structure played a significant role during stable lift-off and near blow-out. In 2006, Su et al. [15] developed a description for flame stabilization which depends on the interaction of the most upstream part of the flame base with the incoming nonreacting jet, this was partly based on premixed flame theory [6] rather than a flamelet quenching model [12]. In 2011, Yoo et al. [16] proposed a stabilization mechanism which is achieved by successive auto-ignition events in hot and fuel-lean mixture where the scalar dissipation rate is low. In 2018, Quattrocchi et al. [17] explained blow-out and lift-off phenomena using the triple flame concept and the balance between the local flow velocity and the flame front velocity or the balance between the scalar dissipation rate and the reaction rate. In 2023, Wang et al. [18], applied premixed flame theory to perform data analysis and claimed that large scale turbulent eddy theory could not predict lift-off height for their specific case study.

1.2. Critical diameter

A key parameter for non-premixed flame stability is critical diameter which represents the minimum nozzle size through which a free jet flame will remain stable at all driving pressures. When hydrogen is released through a nozzle where the diameter is equal or larger than the critical diameter, and it is ignited, the resultant flame is stable regardless of the reservoir pressure, which continuously reduces during emergency blowdown from a storage tank. In 1978, Annushkin and Sverdlov [19] estimated critical diameter for hydrogen as 1.01 mm. They proposed a semi-empirical model to calculate lift-off and blow-out velocity, and considered the stability limit for propane, methane, and hydrogen non-premixed flames. In 1981, Kalghatgi [20] presented a correlation for the blow-out limit of subsonic jet flames, which was extrapolated for chocked flows of fuels including hydrogen. He deduced there is a critical burner diameter above which the flame is stable regardless of gas flow rate. A value was not presented for hydrogen. In 1988, the critical diameter was experimentally determined for natural gas as roughly 30 mm by Birch et al. [21]. For nozzle diameters smaller than the critical value subsonic jet flames were unstable when flow velocity at the nozzle exit exceeded the blow-out velocity; flame re-stabilization was confirmed at elevated driving pressures [21]. In 2002, Devaud et al. [1] performed numerical and experimental studies examining the stability of under-expanded H2–CO flames and compared the results to the work of Kalghatgi [20] and Birch et al. [21]. The critical diameter increased from 1 mm for pure hydrogen to 1.5 mm (corresponding pressure is 1.1 MPa) by adding 4% vol. Of CO [1]. They concluded for their case that RANS was unable to properly capture the turbulent field in under-expanded flows. In 2009, Studer et al. [22] experimentally investigated the diameters close to the critical diameter where stability is restored at 10 bar and 100 bar release pressures for different H_2/CH_4 mixtures. They concluded that these diameters are smaller for the mixtures with higher hydrogen concentration. The critical diameter was not presented for different mixtures. In 2018, Yamamoto et al. [23] presented a flame stability limit curve based on reservoir pressure and nozzle diameter. Whilst they did not use the term critical diameter, it was shown that the nozzle diameter through which the hydrogen jet flame was stable regardless of reservoir pressure was 1.12 mm.

1.3. Experimental studies of hydrogen flame stability

In 1998, Cheng et al. [4] experimentally studied the stability of both

air-diluted and pure subsonic hydrogen diffusion flame in the presence or the absence of coflow air. Results of a pure hydrogen diffusion flame in the still air showed that the lift-off height is independent of nozzle diameter and increased with the velocity at the nozzle exit. In 2009, conditions for a sustained hydrogen flame and blow-out limits were investigated by Mogi et al. [24] through a series of experiments with different nozzle diameters and release pressures. It is this seminal piece of work that is the basis for the numerical study presented here. The limits separating the zones of sustained flame and flame blow-out for hydrogen are defined for low and high pressures limits of hydrogen stable flames. It was concluded that the lower pressure limit for blow-out was almost constant and independent of nozzle diameter, while the upper ("inverted") limit of blow-out pressure limit was reducing with increase of nozzle diameter. The critical diameter was estimated as 1 mm using the graph by Mogi et al. [24]. This was confirmed by the authors through personal communication. In 2013, Hwang et al. [25] experimentally investigated the stability of pure hydrogen flames with co-axial air flow under various fuel velocities and air flow velocities. It was found that flame detachment, lift-off, blow-off and blow-out would occur in the presence of co-axial airflow through nozzle diameters of 3 mm and up to 450 m/s fuel velocity. Results showed that a thicker burner rim would expand the stable region of a sustained attached flame. In 2018, the blow-out process of hydrogen under-expanded jet flames was studied by Yamamoto et al. [23]. It was shown that for stable under-expanded flames, the flame base position is almost constant irrespective of nozzle diameter, but the maximum waistline position, where the radial distance of elliptic stoichiometric contour is a maximum, varies due to Mach disk diameter variation resulting from different reservoir pressures. Thus, the Mach disk variation stemming from the reservoir pressure change, gives rise to different maximum waistline positions. They concluded that, in line with the process proposed in 2006 b y Wu et al. [14], by decreasing the reservoir pressure, the flame base height can exceed the maximum stoichiometric waistline position resulting in the flame blow-out.

1.4. Numerical studies of hydrogen flame stability

The numerical study of hydrogen flame stability limits is challenging as it involves both subsonic and under-expanded hydrogen jets. The shock structure at nozzle exit has been shown to affect flame stability phenomenon in under-expanded jets and thus cannot be neglected as discussed by Yamamoto et al. [23] and Takeno et al. [26]. The complexity of the underlying physical phenomena is not yet fully understood. In 2016, numerical simulations for prediction of hydrogen under-expanded flame lift-off and blow-out were performed by Shentsov et al. [27] using the renormalization group (RNG) k-e turbulence model and eddy dissipation concept (EDC) model for turbulence-chemistry interaction. The results of three cases of 0.3, 0.4, 0.5 mm nozzle diameter and exit pressure of around 11 MPa were presented. Blow-out was observed for 0.3 mm and a stable lifted flame was obtained for 0.4 and 0.5 mm in accordance with experimental data. These results are in line with the stability limits presented by Mogi et al. [24]. The effect of under-expanded jet shock structure was not included in their study, as the real nozzle was replaced by a notional nozzle in simulations. In 2018, Iqbal et al. [28] numerically studied a turbulent hydrogen lifted flame using different turbulent/chemistry interaction models, EDC and Laminar flamelet model, and different turbulent models, RANS, and LES. Scenarios using EDC, RANS and single-step global reaction mechanism as combustion, turbulence and reaction mechanism demonstrated the best agreement to experiments. In 2019, Benim et al. [29] presented a validation study on H2/N2 jet flame to compare different combustion models including composition Probability Density Function transport model, Eddy Dissipation model and Eddy Dissipation Concept using various RANS models. Moreover, different detailed reaction mechanisms, irreversible and reversible single-step reaction mechanisms were assessed. The results demonstrated that the single-step global mechanism of Marinove et al. [30] using the EDC model predicts the value of lift-off height close to experiment. In 2020, Yang et al. [31] investigated premixed hydrogen-air flame stabilization during micro-scale combustion in a swirl micro-combustor through numerical simulation using the realizable k-ε turbulent model and Eddy Dissipation Concept model for turbulent-chemistry interaction. They demonstrated that the flame stability within a micro-combustor would be improved by the method of thermal management, in particular heat recirculation, using a swirl or spiral inlet channels. Also, they concluded combustors made of a material with high thermal conductivity increase the velocity at the swirler inlet section resulting in better preheating performance of reactants and subsequently leading to improvement of flame stability. In 2022, Zhang et al. [32] numerically investigated the effects of combustor structure on hydrogen flame stability in a micro combustor. The recirculation zone and viscous force caused by the bluff body and the high temperature field located behind the bluff body were compared under various inlet velocities, different bluff body width and number of bluff bodies. It was claimed that multiple bluff bodies with a total width of 2 mm and 4 mm or greater demonstrated smaller and higher blow-out limits, respectively. It was concluded that the combustion efficiency would diminish with increase of inlet velocity more slowly for combustor with higher blow out velocity limit.

1.5. Attached flames

When the flame velocity exceeds the local flow velocity in the wake region downstream of the nozzle exit, the flame can propagate upstream through the low-velocity region and become attached to the burner. Consequently, when the flow velocity is higher than the burning velocity in the region close to the burner, the flame is lifted to form a flammable mixture by mixing fuel with entrained air. In 2003, the effect of hydrogen enrichment on methane flame stability was investigated experimentally [33]. The attached flame regime was determined from the lean to rich flammability limit versus inlet flow velocity of the premixed CH4/air. The results showed that the addition of hydrogen extends the methane/air mixture flame stability limits. Similar results were obtained in experiments performed by Wu et al. [34]. In their research, the effect of the addition of propane, methane, and carbon dioxide on the attached hydrogen flame was investigated. The results showed that the addition of propane always caused the attached hydrogen flame to be lifted, but the effect of methane and carbon dioxide addition depends on their concentration, the hydrogen flame may remain attached or lifted. Gao et al. [35] proved that the addition of methane to hydrogen would control burner tip temperature in the case of attached flame and would enhance combustion performance. An et al. [36] experimentally presented hydrogen-methane mixture combustion though a swirl burner to study the flame stabilization modes and flame structure during attached, attached-to-lift-off and lift-off phenomena. It was proposed that there is a linear correlation between the amount of local extinction at the flame base while the flame is attached to the burner and the probability of being in the lift-off state.

Hydrogen attached flames have not been widely investigated, so there is a gap for this topic to clarify under which operating conditions a hydrogen flame is attached to the burner. Attached flames may have adverse effects such as deformation of a burner or structural damage to the burner [35], which is a potential problem. Thus, this topic has been addressed in this paper.

1.6. Importance of the TPRD diameter

For a given tank pressure, there is a clear correlation between the TPRD diameter and flame length, as described by the dimensionless correlation [37]. Indeed [37], discusses how both the TPRD nozzle diameter and shape influences the flame length and width. For example, a TPRD diameter of 5.08 mm with a release from 29.6 MPa will result in a flame of 10.6 m which has clear safety implications [38]. In addition to

leading to unacceptable flame lengths, large TPRD diameters also increase the risk of pressure peaking phenomenon (PPP) in confined spaces. According to Ref. [39], TPRDs with a diameter of 0.5 mm minimize the risks of the pressure peaking phenomenon (the effect of TPRD diameter reduction on potential tank rupture in a fire must be accounted for [40]. On the other hand, the small TPRD diameters (smaller than 1 mm) has the potential for blow-out as discussed in the pervious sections and is shown in the hydrogen flame stability limits graph in section 5.4. H ow ever, a smarter "double-diameter" design for TPRDs might avoid this issue. In 2019 [41], a series of experiments were performed using a "double-diameter" nozzle geometry comprising of two parts, an "upstream" small diameter nozzle, followed by a wider "downstream" nozzle, e.g., 0.5 mm–2 mm. An example is shown later in this paper in Fig. 9. The goal of the work [41] was to determine the under-expanded hydrogen flame length. It was demonstrated [41] that for this 2-part "double-diameter" configuration that if the upstream nozzle diameter is 0.5 mm and the downstream nozzle diameter is larger than 1 mm, the flame would be stable, and blow-out would not happen at pressures that a simple 0.5 mm "single-diameter" nozzle experiences blow-out. More explanation regarding this "double-diameter" nozzle configuration is provided in section 6.2.

1.7. Turbulent Schmidt number

It has been shown that the flame stability behaviour observed in numerical experiments is strongly influenced by simulations parameters. The chemical kinetics model, turbulence-chemistry interaction, and turbulent model constants can all impact ignition characteristics and flame stability behaviour. In 2006, Keistler et al. [42] developed a novel numerical model based on the k-ω turbulent model accounting for variability of turbulent Schmidt, Sc_t, and Prandtl, Pr_t, numbers by adding equations of mass fraction and enthalpy variances and their dissipation rate in order to simulate supersonic hydrogen combustion in a scramjet. The results of the method closely matched experimental results of temperature distribution, prediction of recirculation zones around hydrogen injection location, ignition time, and ignition location. In 2007, Ingenito et al. [43] stated that species fluctuation must be considered in combustion modelling and proposed a constant Sc_t is not valid in supersonic regimes since it does not reproduce turbulent mixing correctly. They simulated a steady flame with $Sc_t = 0.4$ and 0.6, in contrast, $Sc_t = 0.7$ caused flame oscillation [43]. In the next year 2008 Ingenito et al. [44] developed a novel model for supersonic hydrogen combustion in a scramjet by introducing a transport equation for contribution of sub-grid scale kinetic energy and accounted for the effect of species fluctuations on turbulent diffusivity in fine turbulent structures. The model with Sc_t in the range 0.1–0.4 resulted in more stable flames compared to constant $Sc_t = 0.7$ [44]. In 2009 and 2012, El-Amin et al. [45,46] demonstrated that Sc_t is always less than unity since the momentum-transport process is smaller than spreading rate of mass (mass transport) and the assumption of constant Sc_t would imply that momentum transport is similar to mass transport throughout the domain; however it was claimed that the Sc_t decreases from the centreline of the jet radially towards the surrounding air and also different values were observed at different axial positions along the jet trajectory. A constant value of 0.63 was determined for Sc_t based on experimental results obtain by Schefer et al. [47]. In 2012 Xiao et al. [48] followed the same approach as Keistler et al. [42] and showed that for a scheme of variable Sc_t, values of Sc_t can be as low as 0.16 at boundary regions or in mixing layers.

2. Problem description – flame stability

The focus of this study is to validate a numerical model which predicts the critical diameter for hydrogen flames and pressure limits of hydrogen stable flames as a function of nozzle diameter. This model can be used to build the hydrogen flame stability curve for a range of pressures and diameters. Although previous authors [1] were unable to capture the turbulent field in under-expanded flows with RANS, it has been shown here to capture the turbulent flow, lift-off, blow-out, and blow-off behaviour of hydrogen flames by model calibration which is explained in section 5.3. The computational cost was significantly lower compared to our previous LES study [49]. The experimental data of Mogi et al. [24], including the critical diameter based on the flame stability graph, was used to validate the model. Dispersion, and ignition of a constant pressure hydrogen release of 0.2 MPa (gauge) through round nozzles with diameters from 0.8 mm to 2 mm were simulated to investigate critical diameter. A wider range of pressures and diameters were considered to understand flame stability. It should be noted all pressures referred to in this paper are gauge. The releases and geometry (Section 4) were chosen to allow comparison with experimental data. In the experiments, compressed hydrogen gas was ejected horizontally through a circular nozzle. A pilot burner was used to ignite the hydrogen then turned off. Burner location and duration were not given [24]. A pressure transducer on the header measured gauge release pressure (different from stagnant storage pressure).

3. Model and numerical approach

ANSYS Fluent version 20.2 was used as a computational engine to solve the governing equations. A pressure-based solver was applied, and the ideal gas law was used to capture compressibility. The pressure range in this study was lower than 20 MPa and thus real gas effects are deemed negligible. However, several real gas simulations were run to confirm the ideal gas law was an appropriate assumption here, no impact on results was observed and the computational time increased by approximately 20%. The SIMPLE method was used for pressure-velocity coupling. A second-order upwind scheme was used to discretise density, momentum, energy, and species transport equations. A first-order implicit scheme was used for temporal discretisation. A second-order scheme was used to interpolate pressure values at cell faces. The mass, momentum, energy, and species transport equations solved are:

$$\frac{\partial \rho}{\partial t} + \frac{\partial \rho U_i}{\partial x_i} = 0, \tag{1}$$

$$\frac{\partial (\rho U_i)}{\partial t} + \frac{\partial \left(\rho U_i U_j\right)}{\partial x_i} = -\frac{\partial P}{\partial x_i} + \frac{\partial}{\partial x_j}(\mu + \mu_t)\left(\frac{\partial U_i}{\partial x_j} + \frac{\partial U_j}{\partial x_i} - \frac{2}{3}\frac{\partial U_k}{\partial x_k}\delta_{ij}\right) + \rho g_i, \tag{2}$$

$$\frac{\partial (\rho E)}{\partial t} + \frac{\partial}{\partial x_i}(U_i(\rho E + p)) = \frac{\partial}{\partial x_i}\left[\left(k + \frac{\mu_t c_p}{Pr_t}\right)\frac{\partial T}{\partial x_i} - \sum_m h_m\left(- \left(\rho D_m + \frac{\mu_t}{Sc_t}\right)\right) + U_i\,(\mu + \mu_t)\left(\frac{\partial U_i}{\partial x_j} + \frac{\partial U_j}{\partial x_i} - \frac{2}{3}\frac{\partial U_k}{\partial x_k}\delta_{ij}\right)\right] + S_E, \tag{3}$$

$$\frac{\partial (\rho\, Y_m)}{\partial t} + \frac{\partial}{\partial x_i}(\rho U_i Y_m) = \frac{\partial}{\partial x_i}\left[\left(\rho D_m + \frac{\mu_t}{Sc_t}\right)\frac{\partial Y_m}{\partial x_i}\right] + S_m, \tag{4}$$

$$Sc_t = \frac{\mu_t}{\rho D_t} = \frac{\nu_t}{D_t} \tag{5}$$

The Kronecker symbol is defined as

$$\delta_{ij} = \begin{cases} 1 & i = j \\ 0 & i \neq j \end{cases} \tag{6}$$

3.1. Turbulence and combustion simulation approach

The realizable k-$\boldsymbol{\varepsilon}$ turbulence model [50] which is capable of predicting the spreading rate of axisymmetric jets [51] and was applied for simulations of hydrogen under-expanded jet fire by Cirrone et al. [52] was used to solve the turbulent kinetic energy (k) and dissipation rate equations ($\boldsymbol{\varepsilon}$):

$$\frac{\partial(\rho k)}{\partial t}+\frac{\partial}{\partial x_i}(\rho k U_i)=\frac{\partial}{\partial x_i}\left[\left(\mu+\frac{\mu_t}{\sigma_k}\right)\frac{\partial k}{\partial x_i}\right]+G_k+G_b-\rho\varepsilon-Y_M, \tag{7}$$

$$\frac{\partial(\rho \varepsilon)}{\partial t}+\frac{\partial}{\partial x_i}(\rho \varepsilon U_i)=\frac{\partial}{\partial x_i}\left[\left(\mu+\frac{\mu_t}{\sigma_\varepsilon}\right)\frac{\partial \varepsilon}{\partial x_i}\right]+\rho C_1 S_{ij}\varepsilon-\rho C_2\frac{\varepsilon^2}{k+\sqrt{v\varepsilon}}+C_{1\varepsilon}\frac{\varepsilon}{k}C_{3\varepsilon}G_b, \tag{8}$$

$$\mu_t=C_\mu\rho\frac{k^2}{\varepsilon}, \tag{9}$$

where G_k and G_b represent the production of turbulence kinetic energy stemming from mean velocity gradients and buoyancy respectively. Y_M is the contribution of the effects of the fluctuating dilatation dissipation in compressible turbulent flows. σ_k and σ_ε represent turbulent Prandtl numbers for k and ε, corresponding to 1 and 1.2 respectively [51]. $C_{3\varepsilon}$ is calculated as a function of the flow velocity components with respect to the gravitational vector [51]. C_1 is evaluated as a function of the turbulent kinetic energy (k), dissipation rate equations (ε) and the modulus of the mean rate-of-strain tensor, S_{ij} [51]. The turbulent viscosity, μ_t, is computed from equation (9). C_μ is variable and calculated as a function of the turbulent kinetic energy (k), dissipation rate equations (ε), rotation rates, angular velocity of the system rotation and S_{ij} [51]. The EDC model was applied to simulate combustion. EDC is an extension of the eddy dissipation model with treatment of chemical reactions in turbulent flow [53]. One chemical reaction with 4 species was used for the reaction of hydrogen with air, thus water is the only product of the combustion. The source term in equation (4) is the net rate of production of species by chemical reactions defined as [54]:

$$R_m=\frac{\rho(\xi^*)^2}{\tau^*\left[1-(\xi^*)^3\right]}\left(Y_m^*-Y_m\right) \tag{10}$$

Time and length scale of small-scale motions are calculated as per equations (11) and (12) [55]. C_r and C_ξ are time scale and volume fraction constants of 0.4082 and 2.137 [55], R_m is the net rate of production/destruction of species m by chemical reaction, Y_m is species m mass fraction in the surrounding fine-scales state, and Y_m^* is fine-scale mass fraction of species m after reacting over time τ^*:

$$\tau^*=C_\tau\left(\frac{v}{\varepsilon}\right)^{1/2}, \tag{11}$$

$$\xi^*=C_\xi\left(\frac{v\varepsilon}{k^2}\right)^{1/4} \tag{12}$$

4. Numerical details

4.1. Computational domain and mesh

An example of the geometry and nozzle dimensions used in the simulations are shown in Fig. 1. The exit diameter (0.5 mm in Fig. 1) varied with simulations, but all other dimensions remained as shown. The geometry replicates the experimental apparatus apart from two conical conjunction parts which were not detailed [24]. A cylindrical computational domain with a diameter of 6 m and a length of 13 m was considered large enough to eliminate the effect of boundaries on the flame and be applicable to real scenarios.

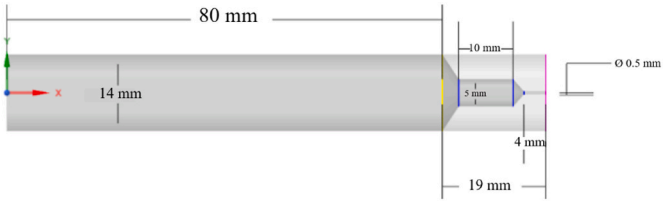

Fig. 1. Sample simulation nozzle geometry for a 0.5 mm nozzle diameter.

Four hexahedral grids were considered for grid independence assessment: “coarse”, “medium”, “fine #1”, and “fine #2”. These comprised roughly 70 k, 200 k, 400 k and 1.5 M control volumes (CVs). The nozzle was resolved by 4, 13, 20 and 26 CVs along the diameter. Minimum CVs are in the nozzle and are 0.025 mm, 0.0076 mm, 0.0050 mm and 0.0038 mm. Minimum CV size for each grid was calculated for the smallest nozzle diameter (0.1 mm). Adequate resolution in the nozzle and vicinity is necessary to resolve the shock structure which was captured in all simulations.

4.2. Boundary and initial conditions

The hydrogen inlet boundary condition was a pressure inlet located 98 mm upstream from the nozzle exit where the pressure transducer in the experiments was mounted. It should be noted that the pressure at the numerical boundary corresponds to the experimentally measured pressure at that point. However, this is not the pressure at the nozzle exit. Fig. 2 illustrates the relationship between pressure at the boundary position and the nozzle exit for the nozzle diameters considered in this work. The pressure at the nozzle exit is linearly proportional to the pressure at the boundary position with a slope of 0.43. This value is affected by pressure losses in the nozzle taken into account during simulations. Indeed, the slope derived using the e-Laboratory Hydrogen Safety [56] for five releases through nozzle diameters of 0.1, 0.3, 0.5, 0.8, and 2 mm at storage pressure range of 0.2–20 MPa is larger, i.e., 0.46. Pressure boundary conditions were applied for the upstream, radial, and downstream boundaries of the domain. Non-reflecting boundary conditions were imposed at the boundaries (inlet and outlet). Hydrogen temperature and mass fraction were 300 K and 1 respectively at the hydrogen inlet boundary. Temperature, absolute pressure, and oxygen mass fraction were 300 K, 0.1 MPa, and 0.23, respectively. Nitrogen mass fraction is defined within Fluent as 0.77. A no-slip condition was employed for all solid wall boundaries. To decrease computational cost, a steady-state solution of the unignited release was first simulated. Once the unignited jet had been established, the transient solution and combustion model was activated. The turbulence model and constants were the same for steady state and unsteady solutions. The pressure-based steady-state solver, the realizable k-ε turbulence model and coupled scheme were used in this initial unignited release stage.

4.3. Ignition simulation

To ignite the hydrogen-air mixture, a static temperature of 2400 K

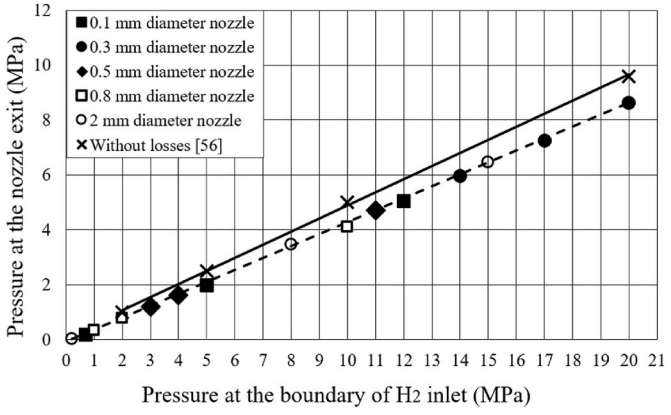

Fig. 2. Variation of the pressure at the nozzle exits with pressure at the boundary position. The solid black line is fitted to predicted data using analytical equation without losses [56], dashed black line is a fitted curve to simulation results considering losses.

was patched in a cube region with dimensions of, e.g., x: 20–40 mm, y: 0–10 mm, and z: 5–10 mm. The ignition source was offset from the central axis of the domain so that flame formation and propagation of the flame back towards the nozzle could be clearly seen. Location of the pilot burner is not given in the experimental study. Care was taken to ensure the ignition source was appropriately located to ensure ignition would occur. Considering hydrogen concentration between the flammability limits and ensuring that the ignition source position does not affect flame extinguishment, the ignition source was located between the maximum stoichiometric waistline position and the nozzle exit. If a flame forms, its base should locate in this region [14,23,26]. According to experimental studies, if the ignition source were to be located where hydrogen axial concentration is less than 11%, the flame may be unstable and propagate downstream when the ignition source is present, or quench when the ignition source is removed [57]. Thus, the position of the numerical ignition source was determined based on the maximum waistline of the stoichiometric hydrogen concentration where it was 29.5% by volume in air, this differed for each diameter and pressure scenario. Water concentration was checked before deactivating the ignition source to ensure the mixture had ignited. Flame behaviour was investigated following removal of the ignition source.

5. Results and discussion

5.1. Grid and time step independence study

A mesh sensitivity study was performed in accordance with the CFD model evaluation protocol [58]. This study is focused on accurate prediction of the critical diameter, which in turn is influenced by both the hydrogen and velocity profiles in the jet prior to ignition. This is further discussed in terms of Sc_t in Section 5.3. Thus, two of the parameters investigated when considering grid independence were the hydrogen concentration and the velocity along the jet axis for the cold flow scenarios prior to ignition. Four grids were compared as noted in Section 4.1. Each grid refinement was defined with respect to the areas of interest including the zone close to nozzle exit where shock structure was captured, and flame anchoring occurred (lift-off distance). As described in Section 1.3 if the flame is stable, the flame base position will be located between the maximum waistline point and nozzle exit [14,23]. Therefore, the number of cells along the nozzle diameter was increased in each stage of refinement and the mesh size was kept almost constant up to the maximum waistline point for each grid where the flame would be anchored. Hydrogen concentration and velocity decay along the central axis obtained from simulation for each grid system were compared and are presented in Fig. 3, for a release from a 1 mm nozzle diameter at 0.2 MPa pressure. Predicted concentration decay, based on the similarity law for hydrogen is included as a means of verification for behaviour downstream in the jet. The similarity law introduced by Chen and Rodi [59] was later expanded and validated for hydrogen expanded and under-expanded jets [37]. Predictions using the velocity decay law [59] are shown too. It should be emphasized that neither the velocity decay law, nor the similarity law are applicable for predictions near the nozzle where the shock structure is present for under-expanded jets. Far field zone from the nozzle is of the most interest from the safety point of view, particularly for definition of hazard distances by flame length. The concentration and velocity decay are:

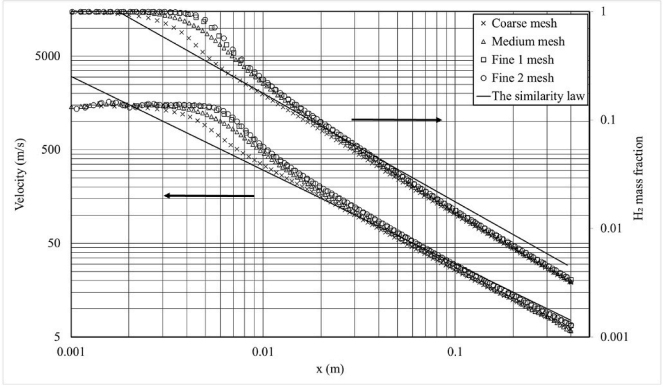

Fig. 3. Hydrogen velocity and mass fraction axial decay for four meshes (release from 0.2 MPa through a 1 mm diameter nozzle).

$$Y_{H_2} = 5.4\sqrt{\frac{\rho_N}{\rho_S}}\,\frac{d}{x}, \tag{13}$$

$$\frac{U}{U_N} = 6.3\sqrt{\frac{\rho_N}{\rho_S}}\,\frac{d}{x}, \tag{14}$$

where ρ_N is hydrogen density at the nozzle exit [37] obtained for a release from a 1 mm nozzle diameter at 0.2 MPa, $\rho_S = 1.20$ kg/m^3 is air density, and V_N is nozzle velocity [37] obtained for the same scenario.

Fig. 3 show that the results of "fine #1" and "fine #2" grids overlap, thus no further refinement was needed. Therefore, "fine #1", the coarser of the two was selected for the study to reduce computational costs. Although "fine #1" grid was selected for the rest of the study, the critical diameter was obtained for the other grids to understand the degree of sensitivity of this parameter to grid resolution. It was confirmed that critical diameters of "course", "medium", "fine #1", and "fine #2" were defined as 0.8, 0.9, 1, and 1 mm, respectively. For a coarser grid both the hydrogen and velocity were found to decay more quickly. Fig. 3 demonstrate that hydrogen concentration decay is shorter, and velocity is lower in the coarse grid in the region close to the nozzle exit (distance from the nozzle exit to maximum waistline location along the axis is up to 35 mm). This is the reason why for a coarser grid a lower value of 0.8 mm was defined as the critical diameter in simulations. The predicted critical diameter increased with grid refinement to 1 mm until no difference was observed between "fine #1" and "fine #2" grids.

An implicit solution scheme was used, and a time-step size independence study was conducted to investigate the accuracy and stability of results. The cold flow simulations were steady state; thus, the time-step independence study was performed for the unsteady ignited stage where a quasi-steady solution had been reached. Temperature as a function of dimensionless axial distance (x/L_f) for a release through a 1 mm nozzle diameter from 0.2 MPa, for four different time-step sizes is shown in Fig. 4. Experimental data for hydrogen flames [37] are included as a means of verification.

Temperature along the axis is the same for time steps of 10^{-4}, 10^{-5}, and 10^{-6} s. The results are clearly different for a time step of 10^{-3} s, where the flame became unstable and was found to numerically blow-out when all scenarios were simulated for 400 ms simulation time. Whilst the results remain similar or "quasi-steady" for the sustained flame cases beyond this time, it is important to note that for the blow-out scenario the temperature will drop with increasing simulation time as the hot products move out of the domain. Temperatures for the scenario with a time step of 10^{-3} s dropped below 1300 K, considered as a flame visibility limit and hot products continue to move downstream, exiting the domain, while temperature in scenarios with time step size of 10^{-4}, 10^{-5}, and 10^{-6} s remained unchanged long enough to demonstrate quasi-steady behaviour of sustained flame. Thus, 10^{-4} s was selected as the most appropriate time step to reduce the computational cost while reproducing accurate results. The adiabatic flame temperature of hydrogen is about 2400 K and higher values are evident in Fig. 4. Possible reasons are the application of a single step reaction mechanism for hydrogen combustion, neglecting the effect of flame radiation, zero response time of "numerical thermocouple", and "numerical pre-heating" of fresh mixture due to the numerical requirement of 3–5 cells to simulate physical discontinuity, etc. The Discrete Ordinates radiation model was investigated. It was found to reduce the flame temperature by approximately 50 K and did not have any effect on flame blow-out or lift-

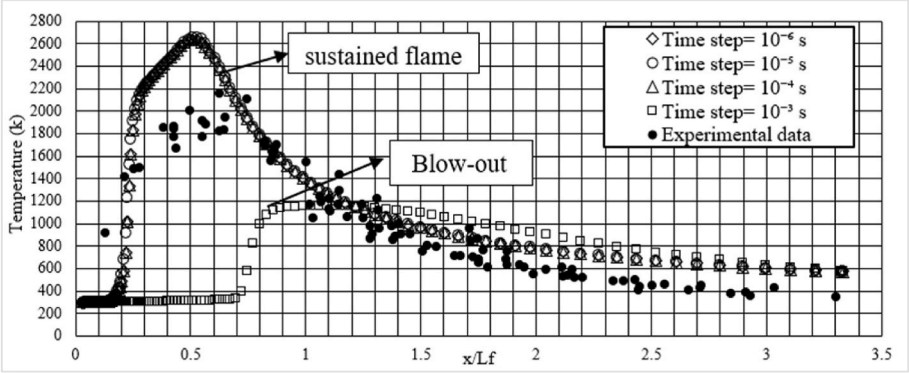

Fig. 4. The temperature along the axis as a function of dimensionless distance by flame length.

off. Thus, it was not included in order to decrease computational costs.

5.2. Blow-out and sustained flames

To demonstrate what was considered as blow-out and a sustained flame in simulations, a comparison of what was observed numerically is presented. The same behaviour was observed in all blow-out cases, which was unlike the behaviour observed for sustained flames. A comparison of a lifted flame and blow-out scenarios based on temperature and water vapour concentration fields is shown in Fig. 5.

The ignition source was applied until the flame can be seen to propagate around the axis and back towards the nozzle. On removal of the ignition source, in the blow-out scenario, a flame was formed, but it moved downstream of the domain and its temperature constantly diminished. In Fig. 5d, the same behaviour could be seen in this scenario for water vapour as the combustion hot product propagating towards the domain exit. Blow-out is shown in Fig. 5b and d for a release pressure of 0.2 MPa and a 0.9 mm diameter nozzle. In the sustained flame scenario with 1.0 mm nozzle diameter and the same pressure, the combustion products region is seen to expand, and a sustained flame is established which remains unchanged after formation, see Fig. 5a. The hot products of combustion, water vapour, confirms the occurrence of sustained flaming as shown in Fig. 5c. The same behaviour is depicted in Fig. 6 for a release from 0.6 mm diameter nozzle at two different pressures 0.1 and 0.06 MPa showing blow-out and a sustained flame, respectively. This figure demonstrates how the flame becomes unstable and blow-out occurs by increasing the pressure from 0.06 MPa to 0.1 MPa. These two scenarios represent behaviour in the region of the lower limit of the flame stability curve which is explained more in section 5.4.

In accordance with definitions of blow-out phenomenon given by Vanquickenborne and Van Tiggelen [6], if the mean velocity of the flow becomes larger than the turbulent flame velocity, flame extinction will finally occur. In 1985 Byggstøyl and Magnussen [60] presented a solution to the fuel concentration transport equation, then following simplifying the solution using k-ε model, they indicated that the turbulent flame propagation velocity is inversely proportional to Sc_t. Based on these works [6,60] it is clear that the relationship between the mean flow velocity and the turbulent burning velocity is key to flame stability. When the mean flow velocity is larger it leads to flame extinction or blow-out. In the present study, different Sc_t numbers, close to the generally accepted constant value of 0.7, were applied in simulations to investigate under which Sc_t number the critical diameter, where sustained flame exists unconditionally for all operating release pressures, fits well the experimental critical diameter of 1 mm measured experimentally [23,24]. In this study it has been found that a decrease in Sc_t is equivalent to a decrease in flow velocity (described further below). As shown in Table 1, the best agreement was achieved for $Sc_t = 0.61$. To determine the critical diameter, a series of simulations for varying nozzle diameter and a release pressure of 0.2 MPa were performed. Starting at 0.8 mm the nozzle diameter was increased in steps of 0.1 mm,

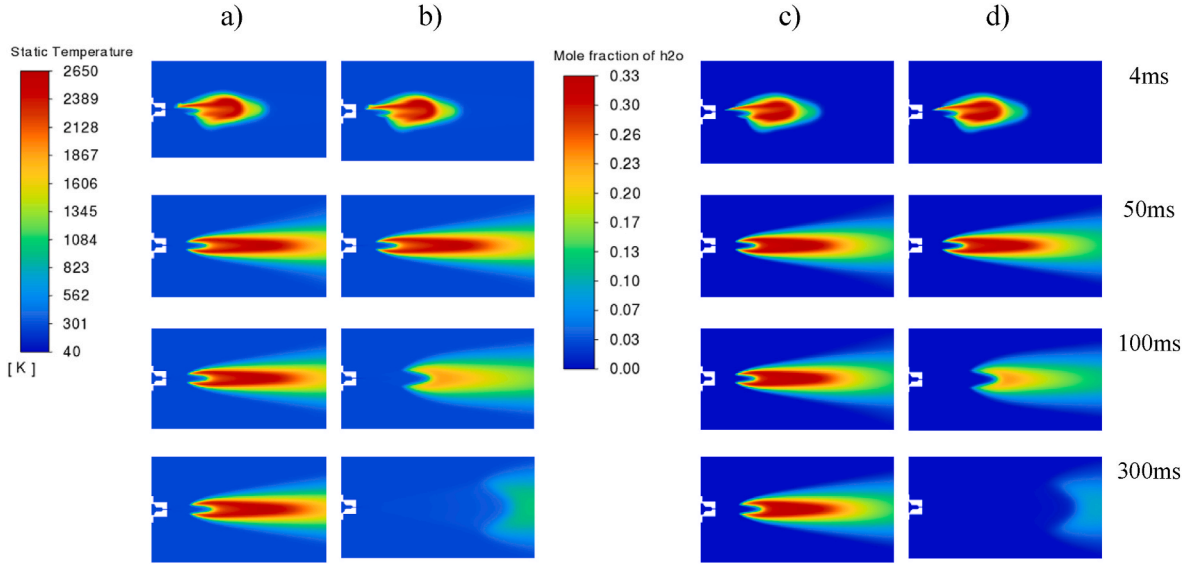

Fig. 5. Sustained flame (a, c) versus blow-out (b, d) for 0.2 MPa driving pressure: a) Temperature (1 mm nozzle); b) Temperature (0.9 mm nozzle); c) Water mole fraction (1 mm nozzle); d) Water mole fraction (0.9 mm nozzle). Note: a cropped computational domain is shown.

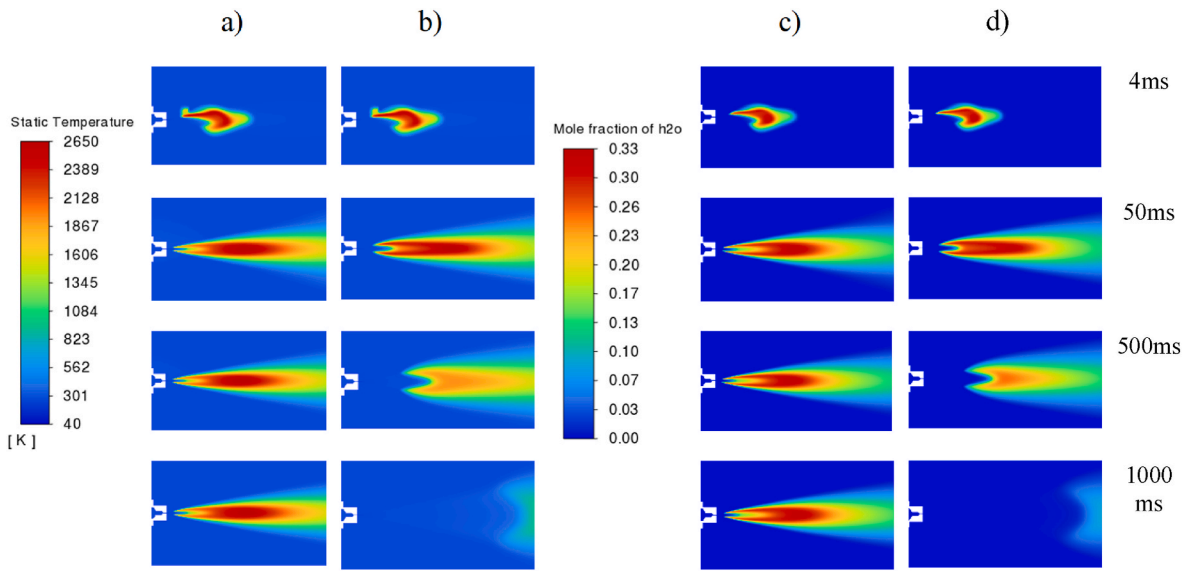

Fig. 6. Sustained flame (a, c) versus blow-out (b, d) through a release from 0.6 mm nozzle diameter: a) Temperature (at 0.06 MPa); b) Temperature (at 0.1 MPa); c) Water mole fraction (0.06 MPa); d) Water mole fraction (0.1 MPa). Note: a cropped computational domain is shown5.3 Effect of turbulent Schmidt number on the critical diameter.

Table 1
Critical diameter for different turbulent Schmidt number compared to experimental value.

	$Sc_t = 0.7$	$Sc_t = 0.61$	$Sc_t = 0.6$	Experiment
Critical diameter	2 mm	1 mm	0.9 mm	1 mm

until a sustained flame was observed. Additional simulations were performed as trials above and below release pressure of 0.2 MPa and resulted in sustained flame at the critical nozzle diameter. The same procedure was followed for $Sc_t = 0.7$ and $Sc_t = 0.6$ and results are shown in Table 1.

As described in Section 5.1, the hydrogen concentration profile in the near nozzle region strongly influences flame stability. By changing Sc_t hydrogen concentration is impacted. For lower Sc_t species mixing is enhanced, and smaller critical diameters are predicted. When concentration profiles for small changes in Sc_t are compared the difference is very small. Hence results of releases with $Sc_t = 0.3$ and $Sc_t = 1.1$ are included here as the difference is more pronounced. The jet with the lower Sc_t has a wider expansion angle. This wider expansion, stemming from the lower Sc_t, leads to greater maximum distance in radial direction perpendicular to nozzle axis on the elliptic stochiometric contour where the flame tip would be anchored (see Fig. 7a), subsequently, as shown in Fig. 7b the flow velocity at this point is almost half the velocity as in the scenario with $Sc_t = 1.1$.

As presented by Vanquickenborne and Van Tiggelen [6], lower flow velocity increases the chance of a sustained flame. Fig. 7a shows hydrogen concentration as a function of radial distance at maximum waistline position for four different Sc_t numbers. In Fig. 7a, horizontal line 29.5% by volume demonstrates the stochiometric hydrogen concentration. The maximum waistline intersected the elliptic stoichiometric contour at radial positions of ±3.8 mm and ±4.7 mm for simulations scenarios with $Sc_t = 1.1$ and $Sc_t = 0.3$ respectively. Cold flow velocity values corresponding to these radial positions are approximately 42 m/s and 22 m/s as indicated in Fig. 7b. Results are shown for relatively high and low Sc_t numbers of 1.1 and 0.3, along with $Sc_t = 0.6$ and $Sc_t = 0.7$ as these are representative of those used in this study. Although the difference for $Sc_t = 0.6$ and $Sc_t = 0.7$ is small, it affects the numerical prediction of critical diameter. The flow velocity for $Sc_t = 0.3$ is smaller, than the case with $Sc_t = 1.1$, as noted by Byggstøyl and Magnussen [60], these two factors lead to a sustained flame and blow-out for the scenarios with $Sc_t = 0.3$ and $Sc_t = 1.1$, respectively. Thus, there is a Sc_t number by which the hydrogen concentration would be reproduced accurately leading to prediction of the correct critical diameter as determined by the experiments. Sc_t represents the ratio between turbulent momentum diffusivity, ν_t, and turbulent mass diffusivity, D_t (see Equations (5) and (9)). For lower Sc_t values turbulent mass transport becomes more significant and outweighs the turbulent momentum diffusion, meaning fuel-air mixing is enhanced,

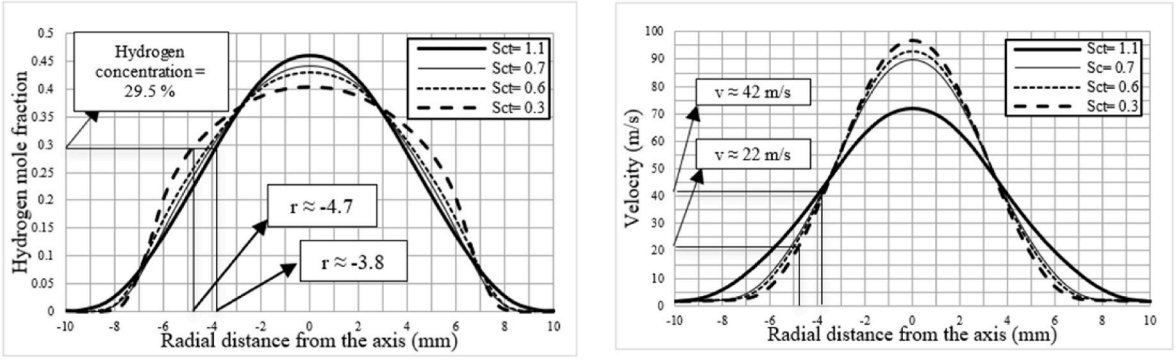

Fig. 7. a) Hydrogen mole fraction and b) velocity as a function of radial distance from the axis at maximum waistline position for four different Sc_t numbers.

increasing the possibility of a sustained flame. Improvement in turbulent mass diffusion, particularly in the mixing layer, where hydrogen meets quiescent surrounding air means the angle of the hydrogen jet spread is augmented. Whilst the focus of this work is on the near nozzle behaviour, and the critical diameter, wider verification of the jet parameters was considered. To verify jet shape, the jet angle was measured and compared with the turbulent free jet angle calculated by Tollmien reported to be 12° for the half-angle [61]. Although the concentration limit for assertion of hydrogen jet boundaries is not a certain value and the release pressure influences density which has effect on jet concentration, the estimated value provided by Tollmien [61] supports the accuracy of the jet profile simulated in this study. Considering 1% as the value of hydrogen mole fraction at the boundaries of a hydrogen jet, the jet half-angle was estimated as 9°, 11°, 12°, and 13°, for Sc_t numbers of 1.1, 0.7, 0.6, and 0.3, respectively. Furthermore, there was no difference between jet half-angles for Sc_t numbers of 0.6 and 0.61 (the last is obtained as the result of the model calibration able to reproduce experimentally observed critical diameter in the simulations). All the jet half-angles will be roughly 1° less if hydrogen mole fraction is equal to 4% at the boundaries of the hydrogen jet.

Flame length and width for the jet released through a 1 mm nozzle at 0.2 MPa with $Sc_t = 0.61$ was compared with data from the literature. Using the dimensionless flame length correlation [37], the conservative flame length for a release through a 1 mm nozzle at 0.2 MPa pressure (gauge) is predicted as 345 mm. The temperature range 1300–1500 K was taken as the visible flame location in the simulations [62] where estimated values for flame length was 319 mm and for flame width 42 mm; a difference of 8% and 5%, compared to flame length and width gained from the correlation and flame width measured in experiments [24], respectively. It should be noted that the flame length and width were almost unaffected by Sc_t number for scenarios with sustained flames as shown in Fig. 8. Note that while flame visibility is generally accepted as being in the range of 1300–1500 K, a value of 1300 K is taken for Fig. 8 as opposed to a range for clarity of presentation. Flame length and width for $Sc_t = 0.3$ was approximately 5% and 2.3% larger than with $Sc_t = 0.61$, respectively. It is worth noting that this is "flame length" from the nozzle exit to the flame tip. Fig. 8 also demonstrates that $Sc_t = 0.61$ results in flame lift-off of 38 mm, while lift-off distance for $Sc_t = 0.3$ is only 12 mm.

5.3. Hydrogen flame stability limit

The model firstly calibrated against the critical diameter was then used to reproduce pressure limits for different nozzle diameters as per the hydrogen flame stability curve by Mogi et al. [24].

The validated model has been used to predict the whole Mogi's curve [24], working with the hypothesis that if a model can reproduce the critical diameter consistent with experiments it will reproduce the stability curve. Examples of simulations run to predict stability limits for two nozzle diameters, i.e., 0.1 mm and 0.3 mm, are given in Table 2 (see also Fig. 9). The points in Fig. 9 represent the stability limit in the upper

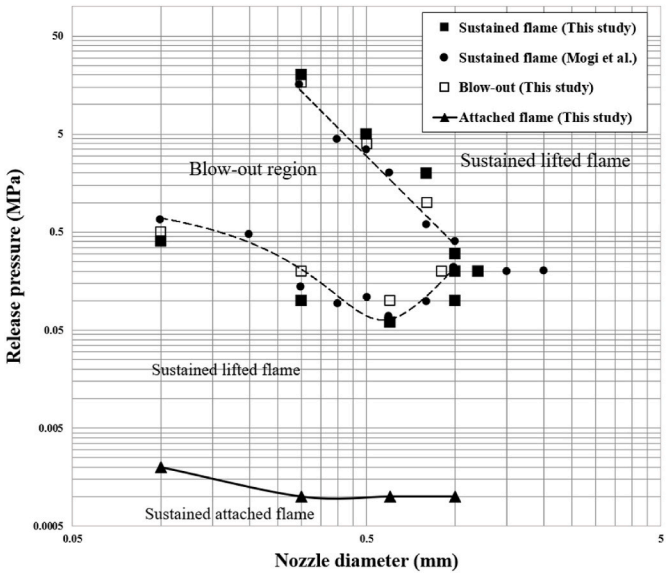

Fig. 9. Hydrogen flame behaviour: including stability limits and attached flame limits.

Table 2
Flame behaviour for simulated releases through 0.1 mm and 0.3 mm diameter nozzles.

Nozzle diameter (mm)	Release pressure (MPa)	Simulated flame status	Experimental flame status
0.3	16	Blow-out	Sustained flame
0.3	17	Blow-out	Sustained flame
0.3	18	Blow-out	Sustained flame
0.3	19	Blow-out	Sustained flame
0.3	20	Sustained flame	Sustained flame
0.1	0.6	Blow-out	Sustained flame
0.1	0.5	Blow-out	Sustained flame
0.1	0.4	Sustained flame	Sustained flame

and lower curves at positions furthest away from the critical diameter. For the lower pressure limit and a 0.1 mm nozzle diameter, a release pressure starting from 0.6 MPa was decreased in steps of 0.1 MPa until a sustained flame was observed. For the upper limit, and a 0.3 mm nozzle diameter, the release pressure was increased from 16 MPa in steps of 1 MPa until a sustained flame was observed. The same procedure was followed for all points represented in Fig. 9 by black and hollow squares for sustained and blow-out scenarios, respectively. Also, at the bottom of the graph, another curve is shown in Fig. 9 which split the sustained flame region at low pressures into attached flames and lifted flames. More explanation is given in section 6.1.

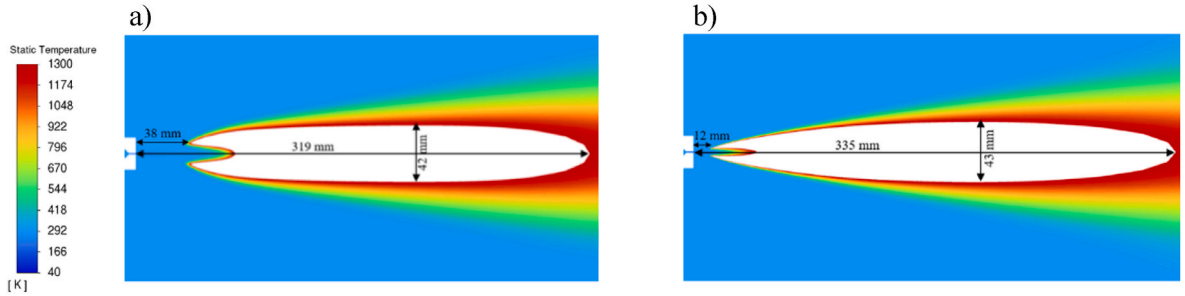

Fig. 8. Temperature contour (truncated domain), clipped to the flame visibility limit of 1300 K for a release through 1 mm nozzle diameter at 0.2 MPa overpressure: a) $Sc_t = 0.61$; b) $Sc_t = 0.3$.

6. Model applications

6.1. Hydrogen attached flames

A sustained flame can be expected for scenarios which are below the lower limit of the flame stability curve of Mogi [24] shown in Fig. 9. Close to the limiting pressure it is expected that a lifted flame will occur. However, as the pressure drops, for a given diameter, the lift-off height of the flame decreases, until the flame eventually becomes attached to the nozzle or burner. An attached flame has implications for nozzle design and may for example cause deformation of a burner nozzle due to high temperature. Thus, understanding the criteria for attached flames is of interest. Therefore, the limits for flame attachment were investigated for several of the nozzle diameters considered previously for flame stability (0.1–1.0 mm). For each diameter, a starting pressure of 0.001 MPa was considered. This was found to give an attached flame in all cases. The pressure was increased gradually (in steps of 0.0001 MPa) until the flame began to detach and became lifted. The maximum pressure that flame was attached to the nozzle is introduced as the limit separating the two states of stable flames for sonic releases.

Fig. 10 demonstrates an attached flame and a lifted flame for a 0.6 mm nozzle at pressures of 0.001 MPa and 0.005 MPa respectively. This defined by simulations pressure limit for attached flames has been added to the flame stability curve for four different diameters to assist with hydrogen safety engineering design. The pressure limits for attached hydrogen flames are shown in Fig. 9 by curve with triangles.

6.2. Inherently safer TPRD design

An inherently safer design for TPRD nozzles that excludes blow-out, mitigates the pressure peaking phenomenon, and reduces flame length is discussed in this section. According to Ref. [39], TPRDs with a diameter of 0.5 mm minimize the risks of pressure peaking phenomenon (PPP). However, based on the hydrogen flame stability limit, for this nozzle dimeter there is possibility for a potential flame to be blow-out in the course of incident. As previously noted, this could lead to hydrogen accumulation for a release in an enclosed space and possible pressure and thermal effects on people and structures in case of deflagration or detonation. To avoid this scenario, the nozzle configuration shown in Fig. 11 is suggested. This nozzle is formed from two parts that are called downstream and upstream nozzles. The diameter of the upstream nozzle is 0.5 mm which controls the mass flow rate, the dominant parameter affecting the PPP, and the diameter of the downstream nozzle is 2 mm (above the critical diameter of 1 mm) which controls the hydrogen concentration and velocity profiles, dominant parameters affecting flame blow-out. Figs. 12 and 13 present the hydrogen concentration and velocity profile at the maximum waistline position for releases from 0.5 mm nozzle diameter and the 0.5 → 2 mm diameter nozzle at 0.2 MPa pressure. The maximum waistline intersected the elliptic stoichiometric contour at radial positions of ±2 mm and ±6.9 mm for releases form 0.5 mm nozzle diameter and "double-diameter" nozzle, respectively. Cold flow velocity values corresponding to these radial positions are approximately 35 m/s and 3 m/s as indicated in Fig. 13. Therefore, the hydrogen concentration profile is changed (becoming wider) when the 2 mm diameter nozzle is located downstream of the 0.5 mm diameter nozzle, and consequently the flow velocity on the elliptic stochiometric contour where the flame tip would be anchored, is decreased dramatically. Hence, a stable flame forms when hydrogen releases through the "double-diameter" nozzle whereas the flame would blow-out if it releases through the 0.5 mm diameter nozzle at the same driving pressure. Four releases from the "double-diameter" 0.5 → 2 mm nozzle and 0.5 mm-diameter nozzle at two different pressures of 0.2 MPa and 2.65 MPa were simulated. The flame was blow-out from the 0.5 mm-diameter nozzle at both pressures and yet was stable from the "double-diameter"

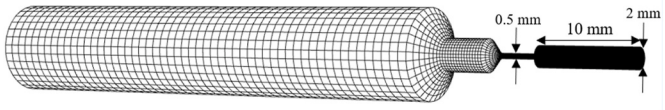

Fig. 11. 3D meshed configuration of "double-diameter" nozzle (0.5 → 2 mm).

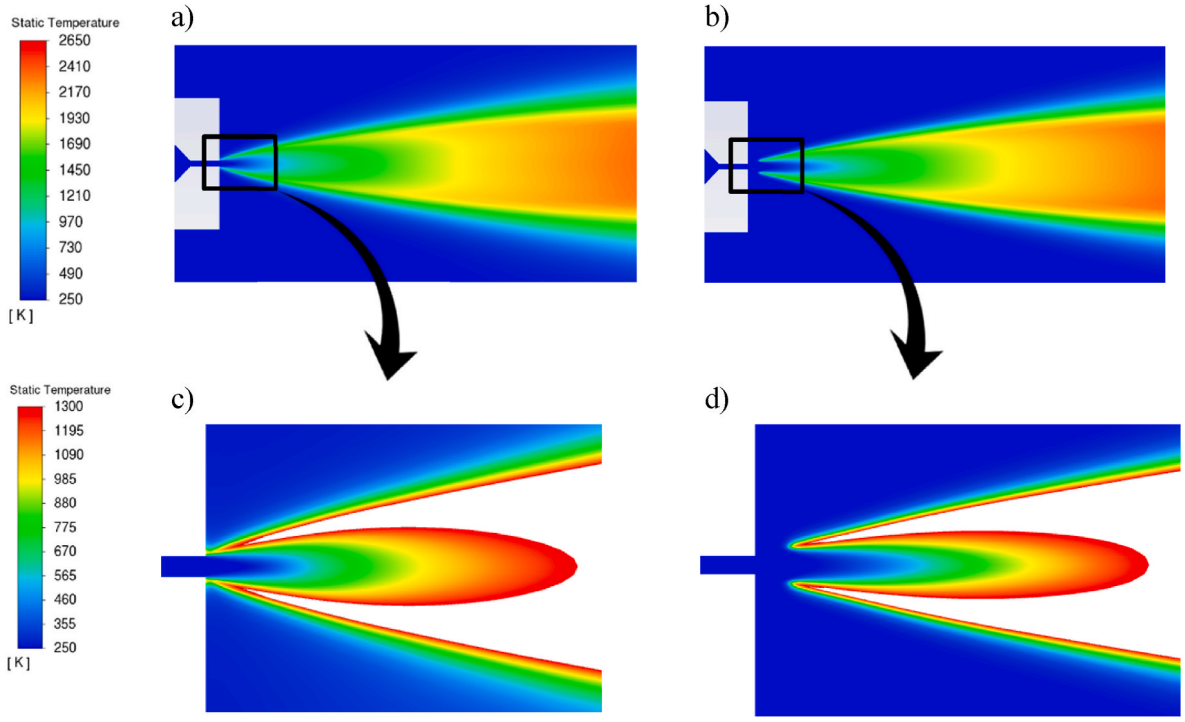

Fig. 10. a) a release from 0.6 mm nozzle diameter nozzle at 0.001 MPa overpressure showing attached flame. b) a release from 0.6 mm nozzle diameter nozzle at 0.005 MPa overpressure showing lifted flame. c) and d) zoomed in view of temperature contour clipped to the flame visibility limit of 1300 K.

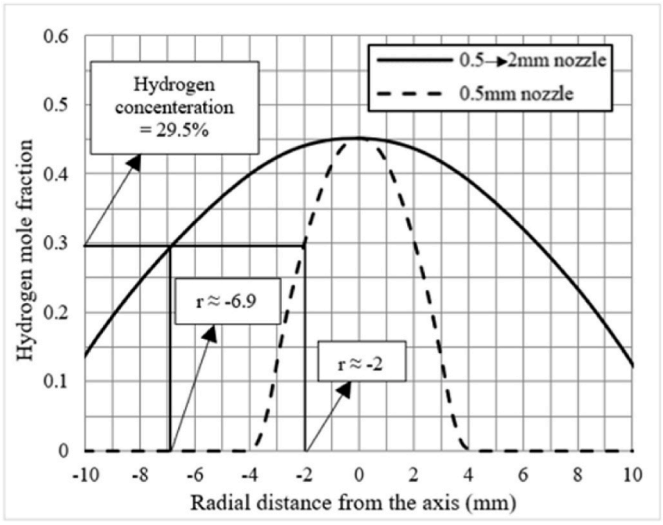

Fig. 12. Hydrogen mole fraction as a function of radial distance at maximum waistline position for nozzle dimeters of 0.5 mm and 0.5 → 2 mm.

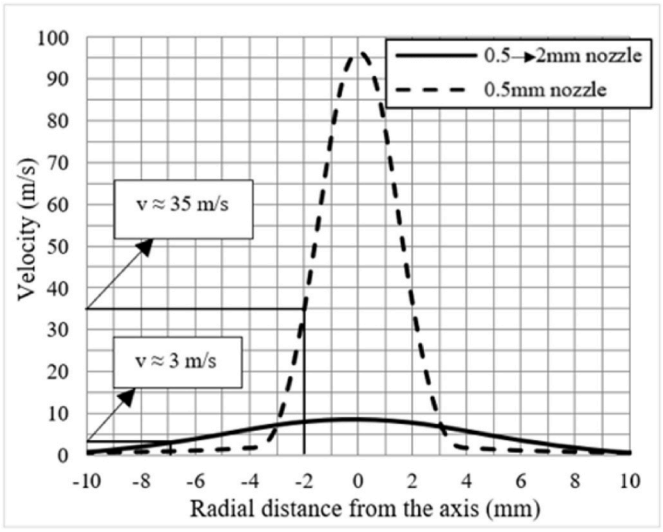

Fig. 13. Velocity as a function of radial distance from the axis at maximum waistline position for nozzle diameters of 0.5 mm and 0.5 → 2 mm.

nozzle.

Fig. 14a shows the sustained flame through the "double-diameter" nozzle at 2.65 MPa pressure. In Fig. 14b, the temperature range is shown to maximum temperature value in the domain up to the flame visibility limit of 1300 K to quantify the lift-off distance (the distance between nozzle exit to visible flame base where temperature is equal to 1300 K). The lift-off distance for a release from a nozzle shape with 0.5 mm upstream nozzle diameter and 2 mm downstream nozzle diameter at pressure 2.65 MPa was measured experimentally by Henriksen et al. [41] as 13 mm. This is in good agreement with the numerically obtained value of 15 mm (acceptable 15% overprediction). Clearly this nozzle design has positive implications for inherently safer TPRD design. It is recommended that this work is considered in the design of TPRDs where the initial nozzle diameter is below the critical diameter for hydrogen of 1 mm.

7. Conclusions

The *originality* of this work includes: (a) numerical prediction of the critical diameter for hydrogen and the insight given on the influence of model parameters on this, (b) numerical prediction of the pressure limits for both attached and lifted-off hydrogen flames, (c) application of the model to explain and underpin the inherently safer TPRD design. The validated against experimental data modelling approach can be used to determine hydrogen flame stability for the whole range of hydrogen storage pressures and nozzle diameters. Sustained flames, blow-out, and blow-off pressure limits as a function of nozzle diameter have all been successfully simulated. Sc_t was shown to affect flame stability. A critical diameter of 1 mm which aligns to that obtained experimentally was reproduced with $Sc_t = 0.61$. Recommendation have been made to improve TPRD design and exclude flame blow-out where the initial release diameter is below the critical diameter for hydrogen of 1 mm.

This study is *significant* for hydrogen safety engineers especially those using CFD models. Understanding of blow-out and blow-off is important for piping and TPRD design. Where blow-out occurs in a confined space there is potential for hydrogen accumulation and formation of a flammable atmosphere. Flame stability should be accounted for in design, and the model described presents a means to do this. The model has been applied to a scenario which demonstrates how blow-out from a TPRD can be avoided, this has clear improved safety implications, particularly in confined spaces. Knowledge of attached flames is useful for lower pressure applications including in a domestic setting.

The *rigour* of this work is in both the validation and verification of the time efficient contemporary CFD model. The simulated critical diameter for hydrogen of 1 mm aligns to that determined in experiments. Results were shown to be grid independent and time step convergent. The model

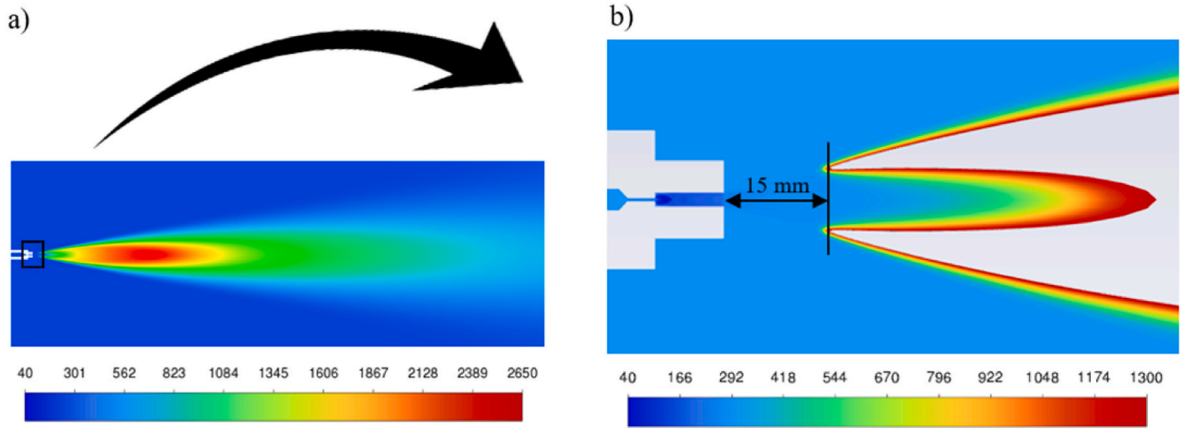

Fig. 14. "Double-diameter" nozzle which eliminates flame blow-out: a) temperature contour showing flame configuration (truncated domain), b) temperature contour clipped to the flame visibility limit of 1300 K showing lift-off distance.

was applied to reproduce pressure limits of flame stability, i.e., Mogi's diagram, for diameters below the critical value. The model is able to reproduce in simulations the experimentally measured flame length and width, jet angle, and flame lift-off.

Declaration of competing interest

The authors declare that they have no known competing financial interests or personal relationships that could have appeared to influence the work reported in this paper.

Acknowledgements

The authors are grateful to the Engineering and Physical Sciences Research Council (EPSRC) of the UK for support through the EPSRC Centre for Doctoral Training in Sustainable Hydrogen "SusHy" (Grant EP/S023909/1) and Tier 2 High-Performance Computing resources provided by the Northern Ireland High-Performance Computing (NI-HPC) facility (grant EP/T022175/1, https://www.ni-hpc.ac.uk/Kelvin 2).

References

[[1]] Devaud CB, Kelman JB, Moss JB, Stewart CD. Stability of underexpanded supersonic jet flames burning H2-CO mixtures. Shock Waves 2002;12(3):241–9. https://doi.org/10.1007/s00193-002-0152-3.
[[2]] Wu Y, Al-Rahbi IS, Lu Y, Kalghatgi GT. The stability of turbulent hydrogen jet flames with carbon dioxide and propane addition. Fuel 2007;86(12–13):1840–8. https://doi.org/10.1016/j.fuel.2006.11.032.
[[3]] Messaoudani ZL, Hamid MD, Wu Y, Hassan CR. Experimental investigation of the flame stability limits for H 2+ C 3 H 8, H 2+ C 2 H 6 and H 2+ CH 4 jet flames. Brazilian Journal of Chemical Engineering 2022;39:487–510. https://doi.org/10.1007/s43153-021-00169-4.
[[4]] Cheng TS, Chiou CR. Experimental investigation on the characteristics of turbulent hydrogen jet flames. Combustion Science and Technology 1998;136 (1–6):81–94. Jul 1, https://doi:10.1080/00102209808924166.
[[5]] Phillips H. Flame in a buoyant methane layer. In: Symposium (international) on combustion. Elsevier; 1965. p. 1277–83. Jan 1;10(1), https://doi:10.1016/S0082-0784(65)80262-4.
[[6]] Vanquickenborne L, Van Tiggelen A. The stabilization mechanism of lifted diffusion flames. Combustion and Flame 1966;10(1):59–69. https://doi.org/10.1016/0010-2180(66)90028-9.
[[7]] Kalaghatigi G. Lift-off heights and visible lengths of vertical turbulent jet diffusion flames in still air. Combustion Science and Technology 1984;41(1–2): 17–28.
[[8]] Kaplan CR, Oran ES, Baek SW. Stabilization mechanism of lifted jet diffusion flames. Symposium (International) on Combustion 1994;25(1):1183–9. https://doi.org/10.1016/S0082-0784(06)80757-5.
[[9]] Joedicke A, Peters N, Mansour M. The stabilization mechanism and structure of turbulent hydrocarbon lifted flames. Proceedings of the Combustion Institute 2005;30(1):901–9. https://doi.org/10.1016/j.proci.2004.08.031.
[[10]] Broadwell JE, Dahm WJA, Mungal MG. Blowout of turbulent diffusion flames. Proceedings of the Twentieth Symposium (International) on Combustion 1984; 20(1):303–10. https://doi.org/10.1016/S0082-0784(85)80515-4.
[[11]] Tieszen SR, Stamps DW, O'Hern TJ. A heuristic model of turbulent mixing applied to blowout of turbulent jet diffusion flames. Combustion and Flame 1996;106(4):442–62. https://doi.org/10.1016/0010-2180(96)00008-9.
[[12]] Peters N, Williams FA. Liftoff characteristics of turbulent jet diffusion flames. AIAA journal 1983;21(3):423–9. https://doi.org/10.2514/3.8089.
[[13]] Müller CM, Breitbach H, Peters N. Partially premixed turbulent flame propagation in jet flames. Symposium (international) on combustion 1994;25(1): 1099–106. https://doi.org/10.1016/S0082-0784(06)80747-2.
[[14]] Wu CY, Chao YC, Cheng TS, Li YH, Lee KY, Yuan T. The blowout mechanism of turbulent jet diffusion flames. Combustion and Flame 2006;145(3):481–94. https://doi.org/10.1016/j.combustflame.2006.01.004.
[[15]] Su LK, Sun OS, Mungal MG. Experimental investigation of stabilization mechanisms in turbulent, lifted jet diffusion flames. Combustion and Flame 2006;144(3):494–512. https://doi.org/10.1016/j.combustflame.2005.08.010.
[[16]] Yoo CS, Richardson ES, Sankaran R, Chen JH. A DNS study on the stabilization mechanism of a turbulent lifted ethylene jet flame in highly-heated coflow. Proceedings of the Combustion Institute 2011;33(1):1619–27. https://doi.org/10.1016/j.proci.2010.06.147.
[[17]] Quattrocchi S, Aggarwal SK, Katta VR. Liftoff and blowout characteristics of laminar syngas nonpremixed flames. International Journal of Hydrogen Energy 2018 Mar 22;43(12):6421–33. https://doi:10.1016/j.ijhydene.2018.01.194.
[[18]] Wang Q, Hu L, Tang F, Palacios A, Chung SH. An experimental study and analysis of lift-off length in inclined nonpremixed turbulent jet flames. Combustion and Flame 2023;255:112855. https://doi.org/10.1016/j.combustflame.2023.112855.
[[19]] Annushkin YM, Sverdlov ED. Stability of submerged diffusion flames in subsonic and underexpanded supersonic gas-fuel streams. Combustion, Explosion and Shock Waves 1978;14:597–605. https://doi.org/10.1007/BF00789718.
[[20]] Kalghatgi GT. Blow-out stability of gaseous jet diffusion flames. Part I: in still air. Combustion Science and Technology 1981;26(5–6):233–9. https://doi.org/10.1080/00102208108946964.
[[21]] Birch AD, Brown DR, Cook DK, Hargrave GK. Flame stability in underexpanded natural gas jets. Combustion Science and Technology 1988;58(4–6):267–80. https://doi.org/10.1080/00102208808923967.
[[22]] Studer E, Jamois D, Jallais S, Leroy G, Hebrard J, Blanchetiere V. Properties of large-scale methane/hydrogen jet fires. International journal of hydrogen energy 2009;34(23):9611–9. https://doi.org/10.1016/j.ijhydene.2009.09.024.
[[23]] Yamamoto S, Sakatsume R, Takeno K. Blow-off process of highly under-expanded hydrogen non-premixed jet flame. International Journal of Hydrogen Energy 2018;43(10):5199–205. https://doi.org/10.1016/j.ijhydene.2018.01.116.
[[24]] Mogi T, Horiguchi S. Experimental study on the hazards of high-pressure hydrogen jet diffusion flames. Journal of Loss Prevention in the Process Industries 2009;22(1):45–51. https://doi.org/10.1016/j.jlp.2008.08.006.
[[25]] Hwang J, Bouvet N, Sohn K, Yoon Y. Stability characteristics of non-premixed turbulent jet flames of hydrogen and syngas blends with coaxial air. International journal of hydrogen energy 2013;38(12):5139–49. https://doi.org/10.1016/j.ijhydene.2013.01.182.
[[26]] Takeno K, Yamamoto S, Sakatsume R, Hirakawa S, Takeda H, Shentsov V, et al. Effect of shock structure on stabilization and blow-off of hydrogen jet flames. International Journal of Hydrogen Energy 2020;45(16):10145–54. https://doi.org/10.1016/j.ijhydene.2020.01.217.
[[27]] Shentsov V, Sakatsume R, Makarov D, Takeno K, Molkov V. Lift-off and blow-out of under-expanded hydrogen jets: experiments versus simulations. In: Proceedings of the 8th international seminar on fire and explosion hazards (ISFEH8). Hefei, China: University of Science and Technology of China; 2016. April 25-28.
[[28]] Iqbal S, Pfeiffelmann B, Benim AC, Joos F. Numerical analysis of lifted hydrogen flame. In: MATEC web of conferences; 2018. https://doi.org/10.1051/matecconf/201824001014. May 21-24; 240(7), Cracow, Poland.
[[29]] Benim AC, Pfeiffelmann B. Validation of combustion models for lifted hydrogen flame. September 3-6;128. In: E3S web of conferences; 2019, 01014. https://doi.org/10.1051/e3sconf/201912801014. Rome, Italy.
[[30]] Marinov NM, Westbrook CK, Pitz WJ. Detailed and global chemical kinetics model for hydrogen. Transport phenomena in combustion 1996;1(118–129):80.
[[31]] Yang X, Yang W, Dong S, Tan H. Flame stability analysis of premixed hydrogen/air mixtures in a swirl micro-combustor. Energy 2020;209:118495. https://doi.org/10.1016/j.energy.2020.118495.
[[32]] Zhang Y, Lu Q, Fan B, Long L, Quaye EK, Pan J. Effect of multiple bluff bodies on hydrogen/air combustion characteristics and thermal properties in micro combustor. International Journal of Hydrogen Energy 2023;48(10):4064–72. https://doi.org/10.1016/j.ijhydene.2022.10.268.
[[33]] Schefer RW. Hydrogen enrichment for improved lean flame stability. International Journal of Hydrogen Energy 2003;28(10):1131–41. https://doi.org/10.1016/S0360-3199(02)00199-4.
[[34]] Wu Y, Lu Y, Al-Rahbi IS, Kalghatgi GT. Prediction of the liftoff, blowout and blowoff stability limits of pure hydrogen and hydrogen/hydrocarbon mixture jet flames. International Journal of Hydrogen Energy 2009;34(14):5940–5. https://doi.org/10.1016/j.ijhydene.2009.01.084.
[[35]] Gao J, Hossain A, Nakamura Y. Flame base structures of micro-jet hydrogen/methane diffusion flames. In: Proceedings of the combustion institute; 2017. p. 4209–16. https://doi.org/10.1016/j.proci.2016.08.034. 36(3).
[[36]] An Q, Steinberg AM. The role of strain rate, local extinction, and hydrodynamic instability on transition between attached and lifted swirl flames. Combustion and Flame 2019;199:267–78. https://doi.org/10.1016/j.combustflame.2018.10.029.
[[37]] Molkov V. In: Fundamentals of hydrogen safety engineering; 2012. www.bookboon.com.2012.
[[38]] Brennan S, Makarov D, Molkov V. LES of high pressure hydrogen jet fire. Journal of Loss Prevention in the Process Industries 2009;22(3):353–9. https://doi.org/10.1016/j.jlp.2008.12.007.
[[39]] Hussein H, Brennan S, Molkov V. Dispersion of hydrogen release in a naturally ventilated covered car park. International Journal of Hydrogen Energy 2020;45 (43):23882–97. https://doi.org/10.1016/j.ijhydene.2020.06.194.
[[40]] Molkov V, Dadashzadeh M, Kashkarov S, Makarov D. Performance of hydrogen storage tank with TPRD in an engulfing fire. International Journal of Hydrogen Energy 2021;46(73):36581–97. https://doi.org/10.1016/j.ijhydene.2021.08.128.
[[41]] Henriksen M, Gaathaug A, Lundberg J. Determination of underexpanded hydrogen jet flame length with a complex nozzle geometry. International Journal of Hydrogen Energy 2019;44(17):8988–96. https://doi.org/10.1016/j.ijhydene.2018.07.019.
[[42]] Keistler PG, Xiaof X, Hassan HA, Rodriguez CG. Simulation of supersonic combustion using variable turbulent Prandtl/Schmidt number formulation. In: 36th AIAA fluid dynamics conference and exhibit. U.S.A.; 2006. p. 2155–67. https://doi.org/10.2514/6.2006-3733. June 5-8; San Francisco, California.
[[43]] Ingenito A, Bruno C. Advance in LES modelling: effect of the turbulent Schmidt number on supersonic regime. In: 43rd AIAA/ASME/SAE/ASEE joint propulsion conference & exhibit; 2007. p. 5633. https://doi.org/10.2514/6.2007-5633. July 8-11; Cincinnati, OH, U.S.A.

[[44]] Ingenito A, Bruno C. Mixing and combustion in supersonic reactive flows. In: 44th AIAA/ASME/SAE/ASEE joint propulsion conference & exhibit; 2008. p. 4574. https://doi.org/10.2514/6.2008-4574. July 21-23; Hartford, CT, USA.
[[45]] El-Amin MF, Kanayama H. Integral solutions for selected turbulent quantities of small-scale hydrogen leakage: a non-buoyant jet or momentum-dominated buoyant jet regime. International Journal of Hydrogen Energy 2009;34(3): 1607–12. https://doi.org/10.1016/j.ijhydene.2008.11.067.
[[46]] El-Amin MF, Sun S. Horizontal H2–air turbulent buoyant jet resulting from hydrogen leakage. International journal of hydrogen energy 2012;37(4): 3949–57. https://doi.org/10.1016/j.ijhydene.2011.04.007.
[[47]] Schefer RW, Houf WG, Williams TC. Investigation of small-scale unintended releases of hydrogen: momentum-dominated regime. International Journal of Hydrogen Energy 2008;33(21):6373–84. https://doi.org/10.1016/j.ijhydene.2008.05.041.
[[48]] Xiao X, Edwards JR, Hassan HA, Cutler AD. Variable turbulent schmidt-number formulation for scramjet applications. AIAA Journal 2012;44(3):593–9. https://doi.org/10.2514/1.15450.
[[49]] Kazemi M, Brennan S, Molkov V. Numerical modelling of sustained hydrogen combustion and flame blow-off from a TPRD. In: Proceedings of the 10th international seminar on fire and explosion hazards (ISFEH10); 2022. May 22-27; Oslo, Norway.
[[50]] Shih TH, Liou WW, Shabbir A, Yang Z, Zhu J. A new k-ϵ eddy viscosity model for high Reynolds number turbulent flows. Computers and Fluids 1995;24(3): 227–38. https://doi.org/10.1016/0045-7930(94)00032-T.
[[51]] ANSYS fluent theory guide. , PA, USA: Ansys Inc. Canonsburg; 2020.
[[52]] Cirrone DMC, Makarov D, Molkov V. Simulation of thermal hazards from hydrogen under-expanded jet fire. International Journal of Hydrogen Energy 2019;44(17):8886–92. https://doi.org/10.1016/j.ijhydene.2018.08.106.
[[53]] Magnussen BF. On the structure of turbulence and a generalized eddy dissipation concept for chemical reaction in turbulent flow. In: 19th aerospace Sciences meeting; 1981. p. 42. https://doi.org/10.2514/6.1981-42. January 12-15; St. Louis, MO, U.S.A.
[[54]] Magnussen BF. Modeling of pollutant formation in gas turbine combustors based on the eddy dissipation concept. Tianjin, China: Eighteenth International Congress on Combustion Engines; 1989.
[[55]] Gran IR, Magnussen BF. A numerical study of a bluff-body stabilized diffusion flame. Part 2. Influence of combustion modeling and finite-rate chemistry. Combustion Science and Technology 1996;119(1–6):191–217. https://doi.org/10.1080/00102209608951999.
[[56]] e-Laboratory of Hydrogen Safety, Jet parameters model, https://elab.hysafer.ulster.ac.uk/; [accessed 15 June 2023].
[[57]] Veser A, Kuznetsov M, Fast G, Friedrich A, Kotchourko N, Stern G, et al. The structure and flame propagation regimes in turbulent hydrogen jets. International Journal of Hydrogen Energy 2011;36(3):2351–9. https://doi.org/10.1016/j.ijhydene.2010.03.123.
[[58]] Baraldi D, Melideo D, Kotchourko A, Ren K, Yanez J, Jedicke O, et al. Development of a model evaluation protocol for CFD analysis of hydrogen safety issues the SUSANA project. International Journal of Hydrogen Energy 2017;42 (11):7633–43. https://doi.org/10.1016/j.ijhydene.2016.05.212.
[[59]] Chen CJ, Rodi W. Vertical turbulent buoyant jets: a review of experimental data. NASA Sti/Recon Technical Report A 1980;80:23073.
[[60]] Byggstoyl S, Magnussen BF. Model for flame extinction in turbulent flow. Turbulent Shear Flows 1985;4:381–95. https://doi.org/10.1007/978-3-642-69996-2_31. September12-14; University of Karlsruhe, Karlsruhe, FRG. Berlin: Springer; 1985.
[[61]] Tollmien W. Berechnung turbulenter ausbreitungsvorgänge. ZAMM-Journal of Applied Mathematics and Mechanics/Zeitschrift für Angewandte Mathematik und Mechanik 1926;6(6):468–78. https://doi.org/10.1002/zamm.19260060604.
[[62]] Schefer R, Houf B, Bourne B, Colton J. Experimental measurements to characterize the thermal and radiation properties of an open-flame hydrogen plume. In: Proceedings of the 15th annual hydrogen conference and hydrogen expo; 2004 April 26.